

# Silver-Nanoparticle-Assisted Modulation of NH<sub>3</sub> Desorption on MIL-101

Suhyeon Park, Mingyu Gu, Yeram Kim, Cheongwon Bae, Duckjong Kim, and Juyeong Kim\*

Cite This: *ACS Omega* 2022, 7, 19484–19490

Read Online

ACCESS |



Metrics &amp; More

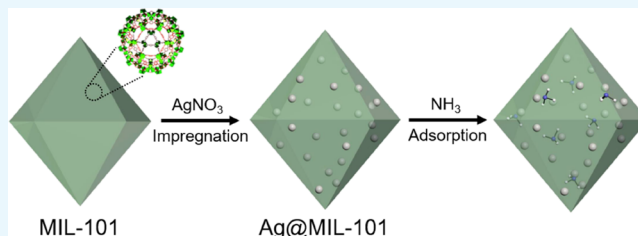


Article Recommendations



Supporting Information

**ABSTRACT:** Ammonia has recently emerged as a promising hydrogen carrier for renewable energy conversion. Establishing a better understanding and control of ammonia adsorption and desorption is necessary to improve future energy generation. Metal–organic frameworks (MOFs) have shown improved ammonia capacity and stability over conventional adsorbents such as silica and zeolite. However, ammonia desorption requires high temperature over 150 °C, which is not desirable for energy-efficient ammonia reuse and recycling. Here, we loaded silver nanoparticles from 6.6 to 51.4 wt% in MIL-101 (Ag@MIL-101) using an impregnation method to develop an efficient MOF-based hybrid adsorbent for ammonia uptake. The incorporation of metal nanoparticles into MIL-101 has not been widely explored for ammonia uptake, even though such hybrid nanostructures have significantly enhanced catalytic activities and gas sensing capacities. Structural features of Ag@MIL-101 with different Ag wt% were examined using transmission electron microscopy, X-ray powder diffraction, and infrared spectroscopy, demonstrating successful formation of silver nanoparticles in MIL-101. Ag@MIL-101 (6.6 wt %) showed hysteresis in the N<sub>2</sub> isotherm and an increase in the fraction of larger pores, indicating that mesopores were generated during the impregnation. Temperature-programmed desorption with ammonia was performed to understand the binding affinity of ammonia molecules on Ag@MIL-101. The binding affinity was the lowest with Ag@MIL-101 (6.6 wt%), including the largest relative fraction in the amount of desorbed ammonia molecules. It was presumed that cooperative interaction between the silver nanoparticle and the MIL-101 framework for ammonia molecules could allow such a decrease in the desorption temperature. Our design strategy with metal nanoparticles incorporated into MOFs would contribute to develop hybrid MOFs that reduce energy consumption when reusing ammonia from storage.



## 1. INTRODUCTION

The demand for ammonia has been growing in various fields such as agriculture,<sup>1</sup> renewable energy conversion,<sup>2,3</sup> and energy conservation.<sup>4,5</sup> Ammonia has largely been traditionally consumed to produce fertilizers as nitrogen suppliers, allowing sufficient food production.<sup>1</sup> It has also recently emerged as a promising hydrogen carrier for renewable energy conversion.<sup>3</sup> Moreover, global climate change demands a paradigm shift to advanced technologies in energy generation, where hydrogen is likely to be a game-changer once its critical pending issues such as green hydrogen production and safe transport are resolved. Because ammonia contains three hydrogen atoms per molecule, it can be considered as an alternative hydrogen source. The storage and transport of ammonia are regarded as more efficient than those of hydrogen because of its high boiling point and facile liquefaction.<sup>6</sup> In terms of energy conservation, industrial cooling systems use ammonia as a working fluid because of its high evaporation enthalpy and vapor pressure.<sup>7</sup> This could improve energy efficiency over the conventional use of hydrofluorocarbon. However, the use of these ammonia-related energy systems is not practical because of a few challenging issues, one of which is the development of a superior adsorbent with high ammonia adsorption capacity

and easy desorption for reuse and recycling.<sup>8</sup> Thus, better understanding and control of ammonia adsorption and desorption would help improve future energy generation and conservation using ammonia.

Metal–organic frameworks (MOFs) have emerged as promising adsorbents for gas capture, catalysis, energy storage, and pollutant separation because of their unique microporosity.<sup>9–13</sup> MOFs are composed of metal ions and organic ligands in a crystalline microporous structure, and they retain high specific surface areas and tunable pore structures. The intrinsic properties and functions of MOFs are improved by modulation of the structural features such as the crystal size and shape as well as composition with heterogeneous components such as metal nanoparticles and polymers.<sup>14–19</sup> For example, the incorporation of silver nanowires with zeolitic

Received: February 26, 2022

Accepted: May 13, 2022

Published: May 27, 2022



imidazolate frameworks allowed an enhancement for electrochemical oxygen evolution by improving electrical conductivity.<sup>15</sup> Such hybrid MOFs with heterogeneous components have shown higher performance than a single MOF entity through synergistic effects, while there are few attempts to utilize the hybrid MOF for ammonia capture and storage to the best of our knowledge.<sup>20,21</sup>

Recent advancements in ammonia uptake have been conducted by developing a MOF structure with improved capacity and stability for ammonia over conventional adsorbents with low ammonia adsorption ( $\sim 11$  mmol/g).<sup>8,22–24</sup> MFM-300(Al) composed of  $[\text{AlO}_4(\text{OH})_2]$  and biphenyl tetracarboxylic acid demonstrated reversible ammonia uptake (15.7 mmol/g) over 50 cycles.<sup>25</sup> Azolate linker-based MOFs with Mn, Co, and Ni could adsorb ammonia up to 15.47 mmol/g and maintain their microporosity under repeated sorption cycles.<sup>22</sup> A series of MIL (MIL: Matériel Institut Lavoisier) displayed a large ammonia uptake of 10 mmol/g with excellent recycling stability.<sup>24</sup> However, ammonia regeneration from MOFs commonly required high thermal energy by heating over 150 °C, which would inevitably entail extra energy consumption in ammonia reuse and recycling.

In this work, we developed MIL-101 nanoparticles impregnated with silver nanoparticles (Ag@MIL-101) to modulate the ammonia desorption temperature of MIL-101 for energy-efficient ammonia reuse. MIL-101 consists of  $\mu_3$ -oxo bridged chromium-trimers with terephthalic acid ligands, and it has a relatively large surface area with hierarchical pore structures and high structural stability against water, oxygen, organic solvents, and heat.<sup>26</sup> Recent reports for high-pressure ammonia adsorption demonstrated that MIL-101 was evaluated as the most stable MOF with higher ammonia uptake than other MOFs (MOF-801, MOF-841, DUT-67, NU-1000, UiO-66, and MIL-100).<sup>7,27</sup> In addition, introducing heterogeneous metal components has shown synergistic effects in gas adsorption and catalysis.<sup>28–33</sup> Noble metals (Pt, Pd, Rh, Au, and Ag) have strong affinity for ammonia,<sup>34</sup> and silver nanoparticles could display increasing selectivity for ammonia sensing on carbon nanotubes.<sup>35</sup> We anticipated that relatively low ammonia desorption energy and cost of Ag among the noble metals would be desirable for the heterogeneous component encapsulated in MIL-101. In Ag@MIL-101, silver ions could be introduced into the micropores of MIL-101 and chemically reduced inside the pores. The adsorption of ammonia molecules was expected to occur inside the micropores of MIL-101 as well as on the surface of silver nanoparticles. An interplay between MIL-101 and silver nanoparticles for holding ammonia could alleviate the ammonia desorption process when 6.6 wt% silver ions were used in Ag@MIL-101.

## 2. EXPERIMENTAL SECTION

**2.1. Chemicals.** Silver nitrate (99.0%,  $\text{AgNO}_3$ , Sigma-Aldrich), sodium borohydride (99%,  $\text{NaBH}_4$ , Sigma-Aldrich), ethyl alcohol (94.5%,  $\text{C}_2\text{H}_5\text{OH}$ , Daejung), chromium nitrate nonahydrate (99%,  $\text{Cr}(\text{NO}_3)_3 \cdot 9\text{H}_2\text{O}$ , Sigma-Aldrich), terephthalic acid (98%,  $\text{C}_8\text{H}_6\text{O}_4$ , Sigma-Aldrich), *N,N*-dimethylformamide (99.8%,  $\text{C}_3\text{H}_7\text{NO}$ , Daejung), methyl alcohol (99.5%,  $\text{CH}_3\text{OH}$ , Daejung), and acetone ( $\text{C}_3\text{H}_6\text{O}$ , 99.8%, Daejung) were purchased and used without further purification. Deionized water (18.2  $\text{M}\Omega \cdot \text{cm}$  at 25 °C) purified using a Merck Millipore Direct Q3 UV Water Purification System was

used for all washing and aqueous solution preparation. All glassware was treated with aqua regia (a mixture of HCl and  $\text{HNO}_3$  with a volume ratio of 3:1), repeatedly washed with deionized water, and dried immediately before use.

**2.2. Synthesis of MIL-101.** MIL-101 nanoparticles were prepared according to a literature method with modification.<sup>36</sup> Deionized water (120 mL) was added to  $\text{Cr}(\text{NO}_3)_3 \cdot 9\text{H}_2\text{O}$  (12.0 g, 30.0 mmol) and terephthalic acid (4.98 g, 30.0 mmol) in a Teflon container, and they were mixed well and sonicated for 20 min. The mixture in the Teflon container was placed in a stainless-steel autoclave and heated in an oven at 218 °C for 18 h. It was then cooled to room temperature for 5 h. A green-colored product was transferred to six 50 mL conical tubes and centrifuged at 5000 rcf for 10 min. The supernatant was discarded as much as possible. The product in each conical tube was dispersed in  $\sim 30$  mL of deionized water and mixed well. The ensuing mixture was centrifuged at 5000 rcf for 10 min, and the supernatant was discarded as much as possible. The product was then dispersed in  $\sim 30$  mL of methyl alcohol and mixed well. The resulting mixture was centrifuged at 5000 rcf for 10 min, and the supernatant was discarded as much as possible. The product was then dispersed in  $\sim 30$  mL of acetone and mixed well. The mixture was centrifuged at 5000 rcf for 10 min, and the supernatant was discarded as much as possible. Finally, the product was collected and dispersed in 120 mL of *N,N*-dimethylformamide and sonicated for 10 min. The mixture was sealed in a glass tube and heated at 70 °C overnight. It was cooled to room temperature and centrifuged at 5000 rcf for 10 min. The product was washed repeatedly with methyl alcohol and acetone. The green wet powder was dried at 75 °C overnight.

**2.3. Synthesis of Ag@MIL-101.** MIL-101 nanoparticles were pretreated in a vacuum oven to remove any solvents and moisture in the MIL-101 pore. They were heated to 200 °C for 6 h under vacuum before silver nanoparticle impregnation. Then, MIL-101 (0.3 g) was dispersed well in ethyl alcohol (33 mL) via ultrasonication. Ethanolic solutions of 0.0333 g for 6.6 wt%, 0.1665 g for 26.1 wt%, and 0.4995 g for 51.4 wt%  $\text{AgNO}_3$  (120 mL) were added to the MIL-101 solution and mixed well under stirring at 300 rpm at room temperature for 5 h and left undisturbed for 3 days for sufficient impregnation. Note that the weight percent of Ag was estimated as dividing the mass of Ag by the mass of MIL-101 in the impregnation reaction. Then, the solution was centrifuged at 5000 rcf for 10 min. The supernatant was then discarded, washed with ethyl alcohol several times, and dried at 80 °C overnight. The dried solids were dispersed in ethyl alcohol (33 mL), and the mixture was added to an ethanolic solution of  $\text{NaBH}_4$  (120 mL) with the same concentration as that of the  $\text{AgNO}_3$  solution under stirring at 300 rpm for 30 min. Then, the solution was centrifuged at 5000 rcf for 10 min, washed with ethyl alcohol twice, and dried under vacuum.

**2.4. Structural Durability Test.** Ag@MIL-101 with Ag 6.6 wt% (0.030 g) was dispersed and sonicated in 3 mL of deionized water, 10  $\mu\text{M}$  HCl, and 10  $\mu\text{M}$  NaOH, respectively. They were left undisturbed at room temperature. In addition, another sample was treated in deionized water at 60 °C. After 4 h, they were centrifuged at 5000 rpm for 10 min, and the supernatant was discarded as much as possible. The product was dispersed in 3 mL of ethyl alcohol. They were centrifuged at 5000 rpm for 10 min, and the supernatant was discarded as much as possible. The product was dried under vacuum for 8 h at room temperature.

**2.5. Characterization.** A JEM-ARM200F Cs-corrected scanning transmission electron microscope (TEM) with a ZrO/W(100) thermal field emission type at 200 kV was used for elemental mapping. An FEI Tecnai TF30ST TEM with a ZrO/W(100) Schottky emitter at 300 kV was used to analyze material morphology. The sample powder was diluted in ethyl alcohol via ultrasonication, and it was dried on a TEM grid (Electron Microscopy Sciences, CF400-CU). A D8 Advanced A25 (BRUKER) was used to measure powder X-ray diffraction (XRD). Fourier-transform infrared spectroscopy (FTIR) was performed using a Nicolet iS5 FTIR spectrometer (Thermo Fisher Scientific) with an iD7 ATR accessory. A BELSORP-mini II (MicrotracBEL) was used to measure the Brunauer–Emmett–Teller (BET) surface area. A TGA Q50 (TA Instruments) was used to perform thermogravimetric analysis (TGA). The sample was heated to 1000 °C by 10 °C/min under nitrogen. An AutoChem 2920 (Micromeritics, USA) was used to measure ammonia temperature-programmed desorption (TPD). Before analysis, the sample was dried in a vacuum oven at 200 °C for 6 h. Then, it was pretreated at 150 °C for 12 h under a helium gas flow. The fraction of ammonia was 15% during adsorption of ammonia at 40 °C for 1 h. The temperature during ammonia desorption was raised to 150 °C by 10 °C/min.

### 3. RESULTS AND DISCUSSION

MIL-101 nanoparticles were prepared through a hydrothermal reaction between chromium nitrate and terephthalic acid (Figure 1).<sup>36</sup> Then, a wet-phase impregnation method was

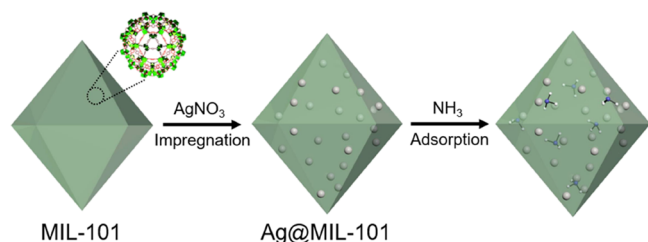


**Figure 1.** Schematics of silver nanoparticle impregnation in MIL-101 for evaluating the adsorption properties of ammonia.

applied to load silver nanoparticles into the micropores of MIL-101. Silver nitrate ions were introduced to MIL-101 nanoparticles dispersed in ethyl alcohol, and they were chemically reduced as silver nanoparticles by sodium borohydride. The amount of silver ions impregnated in MIL-101 was controlled by changing the concentration of silver ions from 0 to 51.4 wt%, from which the amount of silver nanoparticles formed was further characterized using the TEM (Figures 2 and S1). The TEM image of pure MIL-101 displayed octahedral MIL-101 nanoparticles (Figure 2a). After the impregnation and reduction of silver ions inside MIL-101, silver nanoparticles could be well identified by the larger contrast difference in the TEM images (Figure 2b–d). The elemental mapping of Ag@MIL-101 confirmed the presence of silver atoms in MIL-101 (Figure S2). As the concentration of silver ions increased in Ag@MIL-101, more silver nanoparticles were found in the MIL-101 nanoparticles. The sizes of the silver nanoparticles were  $5.1 \pm 3.4$  nm for Ag@MIL-101 (6.6 wt%),  $4.6 \pm 2.7$  nm for Ag@MIL-101 (26.1 wt%), and  $6.9 \pm 4.0$  nm for Ag@MIL-101 (51.4 wt%) (Figure S1). Relatively large and elongated silver nanoparticles could be observed with

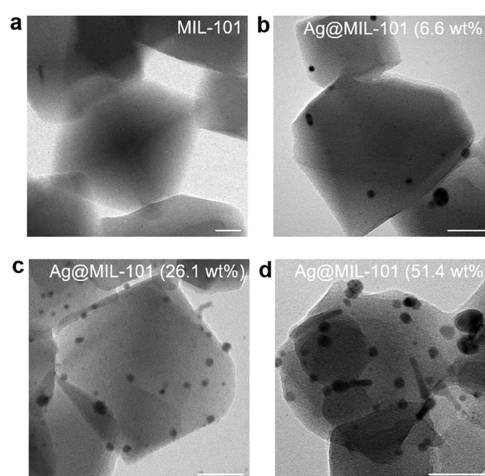


**Figure 2.** TEM images of Ag@MIL-101 with different concentrations of silver ions. (a) 0 wt%, (b) 6.6 wt%, (c) 26.1 wt%, and (d) 51.4 wt%. Scale bar: 100 nm.

Ag@MIL-101 (51.4 wt%), which implied that the amount of silver ions added at 51.4 wt% would overwhelm the restricted spatial volume inside the MIL-101 nanoparticles. In addition, the rather blunt octahedral morphology of Ag@MIL-101 (51.4 wt%) could be attributed to the partial surface degradation of MIL-101 because of the high concentration of sodium borohydride during impregnation. It may appear that any carboxylic acid functional groups undercoordinated in MIL-101 were reacted with sodium borohydride, yielding acyloxyborohydride species.<sup>37</sup>

The crystal structures of Ag@MIL-101 with different Ag wt % values were investigated using the XRD in Figure 3. The

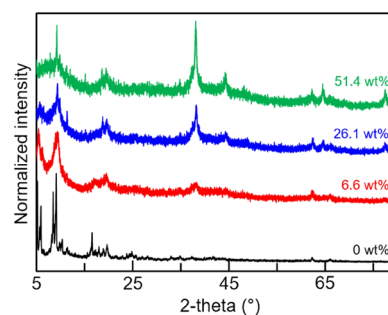


**Figure 3.** Normalized XRD patterns of Ag@MIL-101 with different concentrations of silver ions (black: 0 wt%, red: 6.6 wt%, blue: 26.1 wt%, and green: 51.4 wt%).

XRD patterns of pure MIL-101 showed its characteristic peaks at  $5.3^\circ$  for {511},  $6.0^\circ$  for {531},  $8.5^\circ$  for {822},  $9.1^\circ$  for {753},  $10.4^\circ$  for {1022},  $11.5^\circ$  for {880}, and  $16.6^\circ$  for {1395}, corresponding to the simulated crystal structure of MIL-101.<sup>38</sup> As silver nanoparticles were impregnated in MIL-101, their characteristic signals emerged at  $38.2^\circ$  for Ag {111},  $44.3^\circ$  for Ag {200},  $64.7^\circ$  for Ag {220}, and  $77.4^\circ$  for Ag {311}.<sup>39</sup> The peak intensity values for the silver nanoparticles gradually increased with higher Ag wt% values.

Chemical bonds in Ag@MIL-101 were examined using the FTIR in Figure 4. The vibration modes of terephthalic acid in pure MIL-101 were shown for stretching vibration (C=C) at  $1507\text{ cm}^{-1}$ , symmetric vibration (C–O–C) at  $1396\text{ cm}^{-1}$ , and deformation vibration (C–H) at  $1017$  and  $746\text{ cm}^{-1}$ , and

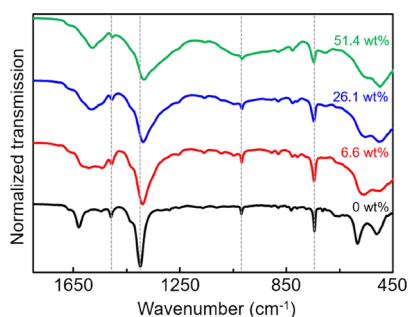


**Figure 4.** Normalized FTIR spectra of Ag@MIL-101 with different concentrations of silver ions (black: 0 wt%, red: 6.6 wt%, blue: 26.1 wt%, and green: 51.4 wt%). The dotted gray lines are visual guides.

adsorbed water molecules in the framework were identified at  $1629\text{ cm}^{-1}$ .<sup>40</sup> Ag@MIL-101 with different Ag wt% values maintained the same vibration modes for terephthalic acid as those observed in pure MIL-101. The characteristic vibration modes for the benzene ring of terephthalic acid in Ag@MIL-101 were positioned at  $1507$ ,  $1017$ , and  $746\text{ cm}^{-1}$ , similar to those in pure MIL-101. In contrast, the symmetric vibration mode for the carboxylate of terephthalic acid at  $1396\text{ cm}^{-1}$  shifted to lower wavenumbers with higher Ag wt% values in Ag@MIL-101:  $1391\text{ cm}^{-1}$  for Ag 6.6 wt%,  $1386\text{ cm}^{-1}$  for Ag 26.1 wt%, and  $1383\text{ cm}^{-1}$  for Ag 51.4 wt%. Such redshifts were attributable to the changes in the coordination modes between the chromium metal center and the ligand in the framework upon the formation of silver nanoparticles.<sup>41,42</sup> In addition, X-ray photoelectron spectroscopy (XPS) spectra of Ag@MIL-101 displayed two peaks for Ag3d at  $367.9$  and  $374.0\text{ eV}$  (Figure S3), and the peak intensities increased with higher Ag wt%. Two peaks for Cr2p were shown at  $576.9$  and  $586.6\text{ eV}$  in pure MIL-101. There was a slight increase in the Cr2p peaks to  $577.2$  and  $586.8\text{ eV}$  in Ag@MIL-101 (51.4 wt%), supporting our IR analysis.

The porous properties of Ag@MIL-101 with different Ag wt% values were examined using  $\text{N}_2$  adsorption and desorption measurements (Figure 5). The BET surface area of pure MIL-

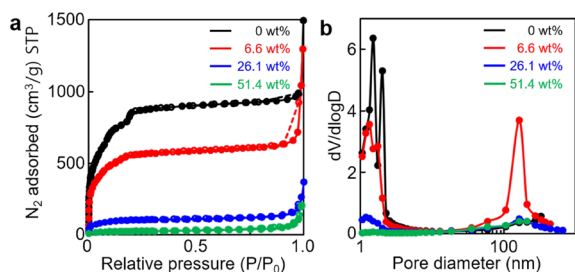


**Figure 5.** (a)  $\text{N}_2$  isotherm plots of Ag@MIL-101 with different concentrations of silver ions (black: 0 wt%, red: 6.6 wt%, blue: 26.1 wt%, and green: 51.4 wt%) for adsorption (filled circle) and desorption (unfilled circle). (b) Pore size distribution of Ag@MIL-101 with different concentrations of silver ions (black: 0 wt%, red: 6.6 wt%, blue: 26.1 wt%, and green: 51.4 wt%).

101 was estimated as  $2462\text{ m}^2/\text{g}$ , and the BET surface area of Ag@MIL-101 gradually decreased as silver nanoparticles were impregnated in MIL-101:  $1774\text{ m}^2/\text{g}$  for Ag 6.6 wt%,  $328\text{ m}^2/\text{g}$  for Ag 26.1 wt%, and  $80\text{ m}^2/\text{g}$  for Ag 51.4 wt%. It was assumed that the impregnated silver nanoparticles could occupy and reduce the micropores in MIL-101, and the heavy atomic

weight of Ag also contributed to such a decrease in the surface area per sample mass. Unlike Ag@MIL-101 with the other Ag wt% values, the  $\text{N}_2$  isotherm of Ag@MIL-101 at 6.6 wt% exhibited hysteresis during desorption at high relative pressures, which could indicate that a certain amount of mesopores were generated upon the impregnation of silver nanoparticles in MIL-101. In addition, the pore size distribution supported changes in the porous properties of Ag@MIL-101 with different Ag wt% values (Figure 5b). The pore size distribution of pure MIL-101 displayed a dominant population in the microporous regime. On the other hand, the population of the micropores in Ag@MIL-101 (6.6 wt%) decreased by half, and the fraction of large pores increased sharply. The Ag@MIL-101 with higher Ag wt% values no longer retained the micropores in the framework.

Thermal stability and chemical stability of Ag@MIL-101 were measured using TGA and durability tests under different chemical environments. Ag@MIL-101 with lower Ag wt%, including Ag@MIL-101 (6.6 wt%) impregnated at  $50\text{ }^\circ\text{C}$  (Figure S4), showed similar weight loss patterns to pure MIL-101 (Figure S5). The initial weight loss was associated with release of  $\text{H}_2\text{O}$ , and the MIL-101 framework began to collapse over  $300\text{ }^\circ\text{C}$ . There was less reduction in the weight loss for Ag@MIL-101 with higher Ag wt% (26.1 and 51.4 wt%), indicating a higher portion of Ag content present in the product. Structural durability of Ag@MIL-101 (6.6 wt%) was investigated at different pH values or high temperature (Figure S6). After left in each environment for 4 h, Ag@MIL-101 still maintained its crystal structure and chemical bonds.

The binding affinity of ammonia gases to Ag@MIL-101 with different Ag wt% values was measured using the TPD in Figure 6 and S7–S10, and Table S1. The Ag@MIL-101 was

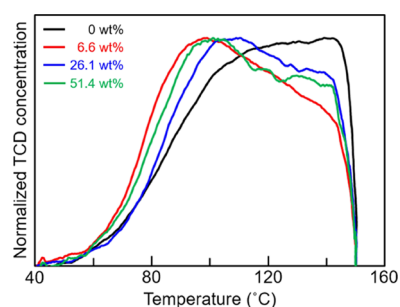


**Figure 6.** Normalized thermal conductivity detector concentration as a function of temperature for ammonia desorption of Ag@MIL-101 with different concentrations of silver ions (black: 0 wt%, red: 6.6 wt%, blue: 26.1 wt%, and green: 51.4 wt%).

pretreated under a flow of helium gas at  $150\text{ }^\circ\text{C}$  for 15 h followed by the adsorption of ammonia molecules to the Ag@MIL-101 at  $40\text{ }^\circ\text{C}$  for 1 h. The strength of the Lewis acidity of Ag@MIL-101 was estimated over a temperature rise to  $150\text{ }^\circ\text{C}$  at  $10\text{ }^\circ\text{C}/\text{min}$ . Two distinct ammonia desorption events with pure MIL-101 were observed at  $115.4\text{ }^\circ\text{C}$  (first ammonia desorption) and  $147.2\text{ }^\circ\text{C}$  (second ammonia desorption). After the impregnation of silver nanoparticles in MIL-101, the first ammonia desorption occurred at lower temperatures at  $99.6\text{ }^\circ\text{C}$  with Ag 6.6 wt%,  $109.5\text{ }^\circ\text{C}$  with Ag 26.1 wt%, and  $104.0\text{ }^\circ\text{C}$  with Ag 51.4 wt%. Likewise, the second ammonia desorption temperature decreased to  $142.1\text{ }^\circ\text{C}$  with Ag 6.6 wt%,  $143.9\text{ }^\circ\text{C}$  with Ag 26.1 wt%, and  $141.9\text{ }^\circ\text{C}$  with Ag 51.4 wt%. The fraction in the amount of the desorbed ammonia molecules at

the first desorption event exceeded that at the second desorption event when silver nanoparticles were introduced in MIL-101.

Presumably, silver nanoparticles provided the adsorption sites with lower binding strength for ammonia than that for the MIL-101 framework. Ag@MIL-101 (6.6 wt%) showed the lowest desorption temperature and the largest relative fraction in the amount of desorbed ammonia at the first desorption event. Such a decrease in the desorption temperature could be attributed to the interplay between the silver nanoparticle surface and the MIL-101 framework. While molecular attraction by the silver nanoparticles would draw ammonia molecules, they could also be attracted by the MIL-101 framework that was exposed physically to the adsorbed ammonia molecules on the silver nanoparticle surface. This adjacent affinity to ammonia appeared to lead to weakening the adsorption energy between ammonia and silver. According to the literature,<sup>35</sup> the binding energy of ammonia on Ag was calculated as 0.40 eV. The binding distance of Ag-NH<sub>3</sub>, 2.301 Å, was longer than that of Cr-NH<sub>3</sub>, 2.157 Å.<sup>43,44</sup> In this respect, the incorporation of silver nanoparticles in MIL-101 was likely to decrease the ammonia desorption temperature. The lowest desorption temperature obtained by Ag@MIL-101 (6.6 wt%) over higher Ag wt% could be attributed to confined pore structure by the MIL-101 framework that may not allow excessive silver nanoparticles to further decrease the ammonia desorption temperature. In addition, ammonia uptake reversibility of Ag@MIL-101 (6.6 wt%) was measured for three cycles of adsorption and desorption. The amount of adsorbed ammonia at the second cycle was reduced by 16% from the first adsorption cycle, and there was a minimal decrease in the third adsorption cycle (Figure S11). The ammonia uptake reversibility in Ag@MIL-101 (6.6 wt%) seemed to be stable after the second cycle. We anticipate that the facile desorption of ammonia from an adsorbent would be beneficial to energy-efficient reuse of stored ammonia molecules.

#### 4. CONCLUSIONS

The MIL-101 nanoparticles impregnated with silver nanoparticles in different quantities were prepared using the hydrothermal reaction and the wet-phase impregnation method. As the amount of silver ions increased from 6.6 to 51.4 wt%, the amount of silver nanoparticles in Ag@MIL-101 was shown to increase using TEM and XPS. Elemental mapping supported the presence of silver nanoparticles in MIL-101. The XRD pattern of Ag@MIL-101 retained the crystallinity of MIL-101, and the intensity for the silver nanoparticles increased in Ag@MIL-101 with higher Ag wt% values. The FTIR spectra of Ag@MIL-101 also maintained the vibration modes of terephthalic acid from the MIL-101 framework. A slight redshift in the symmetric vibration for carboxylate could be attributed to the formation of silver nanoparticles in MIL-101. The BET surface area of Ag@MIL-101 decreased with more silver nanoparticles being impregnated. Particularly, Ag@MIL-101 (6.6 wt%) exhibited hysteresis in the N<sub>2</sub> isotherm and an increase in the fraction of larger pores, implying that mesopores were generated during impregnation. Its structure was maintained at different pH values or temperatures. The binding affinity with ammonia molecules was the lowest with Ag@MIL-101 (6.6 wt%), including the largest relative fraction in the amount of desorbed ammonia molecules. Presumably, the balanced

interplay between the MIL-101 framework and the silver nanoparticles in Ag@MIL-101 (6.6 wt%) could lead to such a decrease in the desorption temperature for ammonia molecules. This would help reduce energy consumption during ammonia reuse from storage.

#### ■ ASSOCIATED CONTENT

##### Supporting Information

The Supporting Information is available free of charge at <https://pubs.acs.org/doi/10.1021/acsomega.2c01171>.

Length distribution of silver nanoparticles in Ag@MIL-101, elemental mapping images, XPS spectra, characterization of Ag@MIL-101 impregnated with AgNO<sub>3</sub> at 50 °C, TGA curves, XRD patterns and IR spectra of Ag@MIL-101 treated in different chemical environments, original TPD plots of MIL-101, original TPD plots of Ag@MIL-101 (6.6 wt%), original TPD plots of Ag@MIL-101 (26.1 wt%), original TPD plots of Ag@MIL-101 (51.4 wt%), TPD plots with three cycles, NH<sub>3</sub> desorption temperature, and the desorbed amount (PDF)

#### ■ AUTHOR INFORMATION

##### Corresponding Author

Juyeong Kim – Department of Chemistry and Research Institute of Natural Sciences, Gyeongsang National University, Jinju 52828, South Korea; [orcid.org/0000-0002-4353-5131](https://orcid.org/0000-0002-4353-5131); Email: [chris@gnu.ac.kr](mailto:chris@gnu.ac.kr)

##### Authors

Suhyeon Park – Department of Chemistry and Research Institute of Natural Sciences, Gyeongsang National University, Jinju 52828, South Korea

Mingyu Gu – Department of Chemistry and Research Institute of Natural Sciences, Gyeongsang National University, Jinju 52828, South Korea

Yeram Kim – Department of Chemistry and Research Institute of Natural Sciences, Gyeongsang National University, Jinju 52828, South Korea

Cheongwon Bae – Department of Chemistry and Research Institute of Natural Sciences, Gyeongsang National University, Jinju 52828, South Korea

Duckjong Kim – Department of Mechanical Engineering, Gyeongsang National University, Jinju 52828, South Korea

Complete contact information is available at:

<https://pubs.acs.org/10.1021/acsomega.2c01171>

##### Notes

The authors declare no competing financial interest.

#### ■ ACKNOWLEDGMENTS

This work was supported by Korea Institute of Energy Technology Evaluation and Planning (grant number: 20192050100060) from the Korea government (MOTIE) and Basic Science Research Program (grant number: 2020R1C1C1007568 and 2021R1A6A3A13044147) through the National Research Foundation of Korea funded by the Ministry of Science, ICT and Future Planning. In addition, this work was partially supported by the KBSI NFEC (grant number: 2019R1A6C1010042) from the Ministry of Education of Korea and Nano-Material Technology Development

Program (grant number: 2009-0082580). We thank Prof. Kiyoung Kwon for use of his furnace oven.

## REFERENCES

- (1) Erisman, J. W.; Sutton, M. A.; Galloway, J.; Klimont, Z.; Winiwarter, W. How a century of ammonia synthesis changed the world. *Nat. Geosci.* **2008**, *1*, 636–639.
- (2) Klerke, A.; Christensen, C. H.; Nørskov, J. K.; Vegge, T. Ammonia for hydrogen storage: challenges and opportunities. *J. Mater. Chem.* **2008**, *18*, 2304–2310.
- (3) Zhang, T.; Miyaoka, H.; Miyaoka, H.; Ichikawa, T.; Kojima, Y. Review on ammonia absorption materials: metal hydrides, halides, and borohydrides. *ACS Appl. Energy Mater.* **2018**, *1*, 232–242.
- (4) Critoph, R. E.; Zhong, Y. Review of trends in solid sorption refrigeration and heat pumping technology. *Proc. Inst. Mech. Eng., Part E* **2005**, *219*, 285–300.
- (5) Saha, B. B.; Uddin, K.; Pal, A.; Thu, K. Emerging sorption pairs for heat pump applications: an overview. *JMST Adv.* **2019**, *1*, 161–180.
- (6) Lan, R.; Irvine, J. T. S.; Tao, S. Ammonia and related chemicals as potential indirect hydrogen storage materials. *Int. J. Hydrogen Energy* **2012**, *37*, 1482–1494.
- (7) Liu, Z.; An, G.; Xia, X.; Wu, S.; Li, S.; Wang, L. The potential use of metal-organic framework/ammonia working pairs in adsorption chillers. *J. Mater. Chem. A* **2021**, *9*, 6188–6195.
- (8) Kim, D. W.; Kang, D. W.; Kang, M.; Lee, J.-H.; Choe, J. H.; Chae, Y. S.; Choi, D. S.; Yun, H.; Hong, C. S. High ammonia uptake of a metal-organic framework adsorbent in a wide pressure range. *Angew. Chem., Int. Ed.* **2020**, *59*, 22531–22536.
- (9) Furukawa, H.; Cordova Kyle, E.; O’Keeffe, M.; Yaghi Omar, M. The chemistry and applications of metal-organic frameworks. *Science* **2013**, *341*, No. 1230444.
- (10) Hong, D. H.; Shim, H. S.; Ha, J.; Moon, H. R. MOF-on-MOF architectures: applications in separation, catalysis, and sensing. *Bull. Korean Chem. Soc.* **2021**, *42*, 956–969.
- (11) Tasleem, S.; Tahir, M.; Khalifa, W. A. Current trends in structural development and modification strategies for metal-organic frameworks (MOFs) towards photocatalytic H<sub>2</sub> production: A review. *Int. J. Hydrogen Energy* **2021**, *46*, 14148–14189.
- (12) Lee, J.; Hong, S.; Lee, J.; Kim, S.; Kim, J.; Kim, M. Strategies in metal-organic framework-based catalysts for the aerobic oxidation of alcohols and recent progress. *Bull. Korean Chem. Soc.* **2021**, *42*, 359–368.
- (13) Zhou, Y.; Abazari, R.; Chen, J.; Tahir, M.; Kumar, A.; Ikreedeegh, R. R.; Rani, E.; Singh, H.; Kirillov, A. M. Bimetallic metal-organic frameworks and MOF-derived composites: Recent progress on electro- and photoelectrocatalytic applications. *Coord. Chem. Rev.* **2022**, *451*, No. 214264.
- (14) Sun, W.; Zhai, X.; Zhao, L. Synthesis of ZIF-8 and ZIF-67 nanocrystals with well-controllable size distribution through reverse microemulsions. *Chem. Eng. J.* **2016**, *289*, 59–64.
- (15) Wang, Y.; Zhao, M.; Zhao, Q.; Li, Q.; Pang, H. Facile synthesis of silver nanowire-zeolitic imidazolate framework 67 composites as high-performance bifunctional oxygen catalysts. *Nanoscale* **2018**, *10*, 15755–15762.
- (16) Jin, P.; Tan, W.; Huo, J.; Liu, T.; Liang, Y.; Wang, S.; Bradshaw, D. Hierarchically porous MOF/polymer composites via interfacial nanoassembly and emulsion polymerization. *J. Mater. Chem. A* **2018**, *6*, 20473–20479.
- (17) Li, W.; Liu, Y.-Y.; Bai, Y.; Wang, J.; Pang, H. Anchoring ZIF-67 particles on amidoximerized polyacrylonitrile fibers for radionuclide sequestration in wastewater and seawater. *J. Hazard. Mater.* **2020**, *395*, No. 122692.
- (18) Zheng, S.; Sun, Y.; Xue, H.; Braunstein, P.; Huang, W.; Pang, H. Dual-ligand and hard-soft-acid-base strategies to optimize metal-organic framework nanocrystals for stable electrochemical cycling performance. *Natl. Sci. Rev.* **2021**, No. nwab197.
- (19) Geng, P.; Wang, L.; Du, M.; Bai, Y.; Li, W.; Liu, Y.; Chen, S.; Braunstein, P.; Xu, Q.; Pang, H. MIL-96-Al for Li-S batteries: shape or size? *Adv. Mater.* **2022**, *34*, No. 2107836.
- (20) Vikrant, K.; Kumar, V.; Kim, K.-H.; Kukkar, D. Metal-organic frameworks (MOFs): potential and challenges for capture and abatement of ammonia. *J. Mater. Chem. A* **2017**, *5*, 22877–22896.
- (21) Kang, D. W.; Ju, S. E.; Kim, D. W.; Kang, M.; Kim, H.; Hong, C. S. Emerging porous materials and their composites for NH<sub>3</sub> gas removal. *Adv. Sci.* **2020**, *7*, No. 2002142.
- (22) Rieth, A. J.; Tulchinsky, Y.; Dincă, M. High and reversible ammonia uptake in mesoporous azolate metal-organic frameworks with open Mn, Co, and Ni sites. *J. Am. Chem. Soc.* **2016**, *138*, 9401–9404.
- (23) Rieth, A. J.; Dincă, M. Controlled gas uptake in metal-organic frameworks with record ammonia sorption. *J. Am. Chem. Soc.* **2018**, *140*, 3461–3466.
- (24) Chen, Y.; Zhang, F.; Wang, Y.; Yang, C.; Yang, J.; Li, J. Recyclable ammonia uptake of a MIL series of metal-organic frameworks with high structural stability. *Microporous Mesoporous Mater.* **2018**, *258*, 170–177.
- (25) Godfrey, H. G. W.; da Silva, I.; Briggs, L.; Carter, J. H.; Morris, C. G.; Savage, M.; Easun, T. L.; Manuel, P.; Murray, C. A.; Tang, C. C.; Frogley, M. D.; Cinque, G.; Yang, S.; Schröder, M. Ammonia storage by reversible host-guest site exchange in a robust metal-organic framework. *Angew. Chem., Int. Ed.* **2018**, *57*, 14778–14781.
- (26) Férey, G.; Mellot-Draznieks, C.; Serre, C.; Millange, F.; Dutour, J.; Surblé, S.; Margiolaki, I. A chromium terephthalate-based solid with unusually large pore volumes and surface area. *Science* **2005**, *309*, 2040–2042.
- (27) An, G.; Xia, X.; Wu, S.; Liu, Z.; Wang, L.; Li, S. Metal-organic frameworks for ammonia-based thermal energy storage. *Small* **2021**, *17*, No. 2102689.
- (28) Hermannsdörfer, J.; Kempe, R. Selective palladium-loaded MIL-101 catalysts. *Chem. – Eur. J.* **2011**, *17*, 8071–8077.
- (29) Dai, H.; Cao, N.; Yang, L.; Su, J.; Luo, W.; Cheng, G. AgPd nanoparticles supported on MIL-101 as high performance catalysts for catalytic dehydrogenation of formic acid. *J. Mater. Chem. A* **2014**, *2*, 11060–11064.
- (30) Mao, P.; Qi, B.; Liu, Y.; Zhao, L.; Jiao, Y.; Zhang, Y.; Jiang, Z.; Li, Q.; Wang, J.; Chen, S.; Yang, Y. Ag<sup>II</sup> doped MIL-101 and its adsorption of iodine with high speed in solution. *J. Solid State Chem.* **2016**, *237*, 274–283.
- (31) Saeed Baamran, K.; Tahir, M. Thermodynamic investigation and experimental analysis on phenol steam reforming towards enhanced H<sub>2</sub> production over structured Ni/ZnTiO<sub>3</sub> nanocatalyst. *Energy Convers. Manage.* **2019**, *180*, 796–810.
- (32) Tahir, M. Well-designed ZnFe<sub>2</sub>O<sub>4</sub>/Ag/TiO<sub>2</sub> nanorods heterojunction with Ag as electron mediator for photocatalytic CO<sub>2</sub> reduction to fuels under UV/visible light. *J. CO<sub>2</sub> Util.* **2020**, *37*, 134–146.
- (33) Muhammad, A.; Tahir, M.; Al-Shahrani, S. S.; Mahmood Ali, A.; Rather, S. U. Template free synthesis of graphitic carbon nitride nanotubes mediated by lanthanum (La/g-CNT) for selective photocatalytic CO<sub>2</sub> reduction via dry reforming of methane (DRM) to fuels. *Appl. Surf. Sci.* **2020**, *504*, No. 144177.
- (34) de Voors, A. C. A.; Koper, M. T. M.; van Santen, R. A.; van Veen, J. A. R. The role of adsorbates in the electrochemical oxidation of ammonia on noble and transition metal electrodes. *J. Electroanal. Chem.* **2001**, *506*, 127–137.
- (35) Cui, S.; Pu, H.; Lu, G.; Wen, Z.; Mattson, E. C.; Hirschmugl, C.; Gajdardziska-Josifovska, M.; Weinert, M.; Chen, J. Fast and selective room-temperature ammonia sensors using silver nanocrystal-functionalized carbon nanotubes. *ACS Appl. Mater. Interfaces* **2012**, *4*, 4898–4904.
- (36) Bromberg, L.; Diao, Y.; Wu, H.; Speakman, S. A.; Hatton, T. A. Chromium(III) terephthalate metal organic Framework (MIL-101): HF-free synthesis, structure, polyoxometalate composites, and catalytic properties. *Chem. Mater.* **2012**, *24*, 1664–1675.

(37) Jones, J. C. Transition metals as structural components in the construction of molecular containers. *Chem. Soc. Rev.* **1998**, *27*, 289–300.

(38) Minh Thanh, H. T.; Thu Phuong, T. T.; Le Hang, P. T.; Tam Toan, T. T.; Tuyen, T. N.; Mau, T. X.; Khieu, D. Q. Comparative study of Pb(II) adsorption onto MIL-101 and Fe-MIL-101 from aqueous solutions. *J. Environ. Chem. Eng.* **2018**, *6*, 4093–4102.

(39) Anandalakshmi, K.; Venugobal, J.; Ramasamy, V. Characterization of silver nanoparticles by green synthesis method using *Petalium murex* leaf extract and their antibacterial activity. *Appl. Nanosci.* **2016**, *6*, 399–408.

(40) Liu, Q.; Ning, L.; Zheng, S.; Tao, M.; Shi, Y.; He, Y. Adsorption of carbon dioxide by MIL-101(Cr): regeneration conditions and influence of flue gas contaminants. *Sci. Rep.* **2013**, *3*, 2916.

(41) Wang, Q.; Shao, L.; Ma, Z.; Xu, J.; Li, Y.; Wang, C. Hierarchical porous PANI/MIL-101 nanocomposites based solid-state flexible supercapacitor. *Electrochim. Acta* **2018**, *281*, 582–593.

(42) Lu, Y.; Yue, C.; Liu, B.; Zhang, M.; Li, Y.; Yang, W.; Lin, Y.; Pan, Y.; Sun, D.; Liu, Y. The encapsulation of POM clusters into MIL-101(Cr) at molecular level: LaW10O36@MIL-101(Cr), an efficient catalyst for oxidative desulfurization. *Microporous Mesoporous Mater.* **2021**, *311*, No. 110694.

(43) El Aribi, H.; Rodriguez, C. F.; Shoeib, T.; Ling, Y.; Hopkinson, A. C.; Siu, K. W. M. Threshold collision-induced dissociation determination and molecular orbital calculations of the binding energies of sodium and silver ions to small nitrogen-containing ligands. *J. Phys. Chem. A* **2002**, *106*, 8798–8805.

(44) Kozubal, J.; Heck, T. R.; Metz, R. B. Vibrational spectroscopy of  $\text{Cr}^+(\text{NH}_3)_n$  ( $n = 1-6$ ) reveals coordination and hydrogen-bonding motifs. *J. Phys. Chem. A* **2019**, *123*, 4929–4936.